Testing and performance of IFS upgrades to GPI 2.0

Dillon Peng^a, Jeffrey Chilcote^a, Quinn Konopacky^b, Randall Hamper^a, Joel Burke^a, Brian Sands^c, Matthew Engstrom^c, Abigail Karaszewski^a, Rebecca Boyle^a, Mary Anne Limbach^d, Alexandra Greenbaum^e, Anand Sivaramakrishnan^f, Alexa Rizika^a, Saavidra Perera^b, Clarissa Do Ó^b, Jayke Nguyen^b, Bruce Macintosh^g, Joeleff Fitzsimmons^h, Christian Marois^{h,i}, Fredrik Rantakyrö^j, Arlene Aleman^k, Jérôme Maire^b, Robert De Rosa^l, Emiel Por^f, Dmitry Savransky^m, Meiji Nguyen^f, Marshall Perrin^f, Remi Soummer^f, Laurent Pueyo^f, Bryony Nickson^f, and Eckhart Spaldingⁿ

^aDepartment of Physics and Astronomy, University of Notre Dame, 225 Nieuwland Science Hall, Notre Dame, IN, 46556, USA

^bCenter for Astrophysics and Space Science, University of California San Diego, La Jolla, CA 92093. USA

^cEngineering and Design Core Facility, University of Notre Dame, 626 Flanner Hall, Notre Dame, IN, 46556, USA

^dDepartment of Physics and Astronomy, Texas A&M University, 4242 TAMU, College Station, TX, 77843-4242, USA

^eIPAC, California Institute of Technology, 1200 E California Blvd Pasadena, CA 91125 ^fSpace Telescope Science Institute, Baltimore, MD 21218, USA

gUniversity of California Observatories, 550 Red Hill Rd, Santa Cruz, CA, 95064, USA ^hNational Research Council of Canada Herzberg, 5071 West Saanich Road, Victoria, BC V9E2E7, Canada

ⁱUniversity of Victoria, 3800 Finnerty Road, Victoria, BC, V8P 5C2, Canada ^jGemini Observatory, Casilla 603, La Serena, Chile

^kKavli Institute for Particle Astrophysics and Cosmology, Stanford University, Stanford, CA 94305, USA

¹European Southern Observatory, Alonso de Córdova 3107, Vitacura, Santiago, Chile ^mSibley School of Mechanical and Aerospace Engineering, Cornell University, Ithaca, NY 14853, USA

ⁿThe University of Sydney, Camperdown NSW 2050, Australia

ABSTRACT

The Gemini Planet Imager (GPI), is a facility class instrument for the Gemini Observatory with the primary goal of directly detecting young Jovian planets. After spending 2013 - 2020 at Gemini South, the instrument is currently undergoing maintenance and upgrades before its transition to Gemini North as GPI 2.0. Among the upgrades are significant changes to the Integral Field Spectrograph (IFS), including the installation of new prisms, Lyot stops/apodizers, and filters. The upgrades are expected to improve overall performance in the relevant wavelengths and angular separations needed for GPI 2.0.

Keywords: Gemini Planet Imager, exoplanets, instrumentation, wavefront sensor, detectors, integral field spectrograph

Further author information: (Send correspondence to D.P.)

D.P.: E-mail: dpeng@nd.edu, Telephone: +1 510 585 8805

1. OVERVIEW OF THE IFS

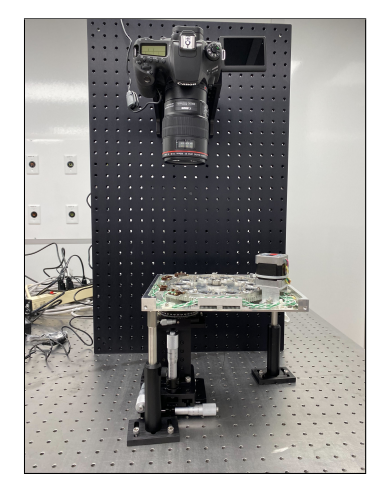
The IFS takes light that has been corrected by the adaptive optics system, removes the unnecessary portions using Lyot stops and apodizers, and then puts the light through a prism and filter to disperse an infrared spectrum on its detector. As the main science instrument of GPI, the IFS is subject to a number of key upgrades affecting nearly all of these aforementioned parts. The first major changes occur at the Lyot wheel, right where light enters the IFS. To improve contrast, new sets of Lyot stops and corresponding apodizers were designed and manufactured, as detailed in Nguyen et al. 2022 [1]. Installation and alignment of these new parts is one of the major challenges faced. Using a decade of performance data from GPI 1.0, we were able to determine that GPI could support a more stringent alignment tolerance for these components. In addition to changing the Lyot stops themselves, the non-redundant apodizer mask (NRM) is being relocated from earlier in the optical path, to the cryogenic Lyot wheel. This change required a redesign and fabrication of the NRM to account for the difference in housing and beam size at its new location. The camera used to align GPI by imaging the pupil plane is being upgraded as well, which will allow for more precise alignment of the system, while also possibly providing room for installation of a new Zernike wavefront sensor to correct for non-common path aberrations.

After the lenslet array, the housing containing the prisms and filters is undergoing major changes as well. The set of prisms, which is responsible for dispersing (or polarizing) the light in the relevant wavelengths, is being changed from a spectral and Wollaston pair to a set of 2 spectral and 1 Wollaston prisms. While the Wollaston prism remains unchanged, both of the spectral prisms are being modified. This change also necessitates a redesign of the mechanism for holding and aligning the prisms, as the previous method was designed specifically to stabilize a set of only 2 prisms. A change of spectral prisms, enables and necessitates change of the filters to adjust the resolution of microspectra on the detector. An additional benefit of these changes is an improvement in throughput performance, which will be discussed later in this paper.

Outside of the IFS itself, some of the peripherals that control and power it are also being changed. With this change comes a shuffling of the arrangement and redesign of the electronics enclosure itself to optimize space and performance.

2. PROCEDURE FOR LYOT STOP AND APODIZER INSTALLATION AND ALIGNMENT

GPI 2.0 has a newly designed set of Lyot stops and apertures which will provide significant throughput improvements, thereby increasing its maximum contrast ratio as well. With a clocking tolerance on the order of 0.01 degrees however, the installation and alignment of these parts must be extremely precise. To do this, the below setup has been constructed.



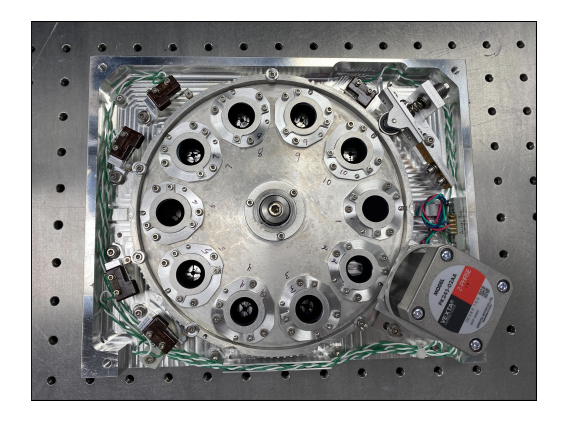


Figure 1. The apparatus for installing and aligning the Lyot stops and apodizers (left), along with a picture of the Lyot wheel itself (right).

The Lyot wheel is raised and level on 3 risers, which are secured to the optics bench. A Canon 90D DSLR camera is suspended above the Lyot wheel, aligned directly to view the opening in the wheel. Below this opening, a movement stage is positioned to be able to move in all 3 dimensions, as well as rotate. A Teflon rod will be secured to this stage, and raised up through the Lyot wheel, where the Lyot stops will then be carefully placed on top. The stage will then be lowered down until the Lyot stop is positioned within the opening, and images will be taken with the DSLR and analyzed to ensure correct positioning. The rotation stage can be used to adjust the clocking of the stop, with a fine adjustment screw allowing for gradual adjustments until analysis of the images confirms proper alignment. The same procedure will be done for the corresponding apodizers in the apodizer wheel as well.

3. CHANGES TO THE NON-REDUNDANT APERTURE MASK

The non-redundant aperture mask (NRM) is a key component of GPI, allowing it to probe small spatial scales at a moderate contrast. The mask itself consists of 10 small pinholes which cause the light passing through to create a specific interference pattern, which can then be measured. Different sources (isolated stars, binary systems, planets, etc.) produce different interference patterns, which can then be identified. Performance of the GPI NRM is analyzed in Greenbaum et al. 2019 [2]. In the original GPI, this mask was located in the aperture wheel; however, for GPI 2.0, the NRM has been moved to the Lyot wheel. Several changes had to be made to account for this shift, regarding the size and shape of the NRM. While the 10 pinhole pattern has been kept the same, the difference in beam size between the aperture and Lyot wheels meant that the pattern and holes had to be adjusted to sit in the beam properly. There is a 17.7% beam size reduction between the pupil plane and the plane of the Lyot wheel, so the pinhole pattern and hole diameters were accordingly reduced; the pinhole sizes were reduced from 0.922 mm to 0.768 mm, while the pattern itself was shrunk down while keeping the relative distances between holes intact.

This part will eventually have to be installed into the Lyot wheel as well; however, its angular tolerance is more lenient than that of the Lyot stops and apodizers.



Figure 2. A manufactured prototype of the new NRM, with reduced dimensions and shaped for the Lyot wheel.

4. IFS PUPIL PLANE CAMERA

Primarily used for ensuring alignment of the system, the IFS pupil plane camera is being upgraded from a Goodrich SU320KTX-1.7 RT to a First Light Imaging C-RED 2. The main benefit of this change is a much higher resolution, allowing for more accurate and precise alignment. However, with improved noise performance as well (analyzed in Peng et al. 2022 [3], there is a new possible use for it. As covered by Chambouleyron et al. 2023 [4], the C-RED 2 could be used as part of a Zernike wavefront sensor to detect non-common path aberrations within the system. The addition of this new NCPA detection method comes as a result of the change from a Shack-Hartmann to a Pyramid WFS design for GPI 2.0.

Table 1. Comparison of the pupil plane camera of GPI 1 and its upgrade; while the Goodrich has a larger physical detector size, the increase in pixel number and decrease in pixel size allows the C-RED 2 to provide a more accurate and precise alignment of the system.

	SU320KTX-1.7RT	C-RED 2
Pixel pitch $(\mu \text{ m})$	40	15
Plane size (pixels)	320×240	640×512
Full Frame Read noise (e^-)	< 50	< 30
Max FPS (full area)	72	600
Non-destructive readout	No	Yes
Variable gain modes	No	Yes

5. CHANGES TO THE IFS PRISMS AND PRISM SLIDE MECHANISM

The IFS prism changes were made to add a new low resolution observation mode, where all bands could be observed simultaneously. The prism designs went though multiple iterations with the initial design being presented in Limbach et al. 2020 [5] and the final resulting prism resolutions being presented in Peng et al. 2022 [3]. The prisms are made of N-SF66/CaF2 materials compared to the GPI 1.0 prisms being made of S-FTM16/BaF2. The new prisms even out the spectral resolutions of the different bands across the board as well, and the reduction in spectral resolution of the K-band from $R \sim 70$ to $R \sim 55$ allows it to be consolidated into a singular band rather than being split between K1 and K2.

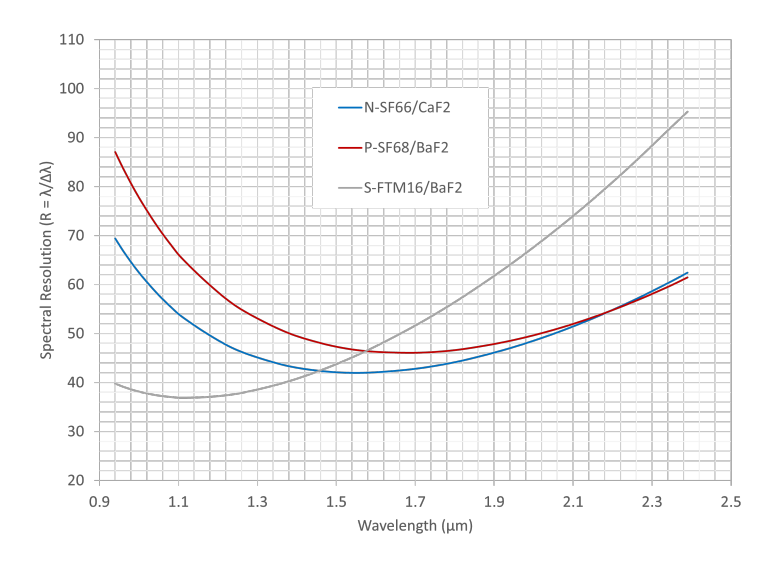


Figure 3. Graph comparing spectral resolution across wavelengths of different material combinations. The new prisms (in blue) provide a smoother overall resolution across all bands compared to the materials of the original GPI prisms (in grey). The red line shows another material combination that was considered.

The mechanism for switching out the IFS prisms must be modified to account for the inclusion of the extra spectral prism for GPI 2.0. The previous method of aligning the 2 prisms involved a rack-and-pinion system as well as magnets on each side to stabilize the prisms. With the addition of the 3rd prism, this method was insufficient, as there would be no way to secure the position of the "middle" prism in the same way the 2 flanking prisms are. As such, the entire mechanism for securing the prism locations has been redesigned, and will completely replace the previous system.

The rack-and-pinion method of translating the prism positions will be replaced by a lead screw driven by a

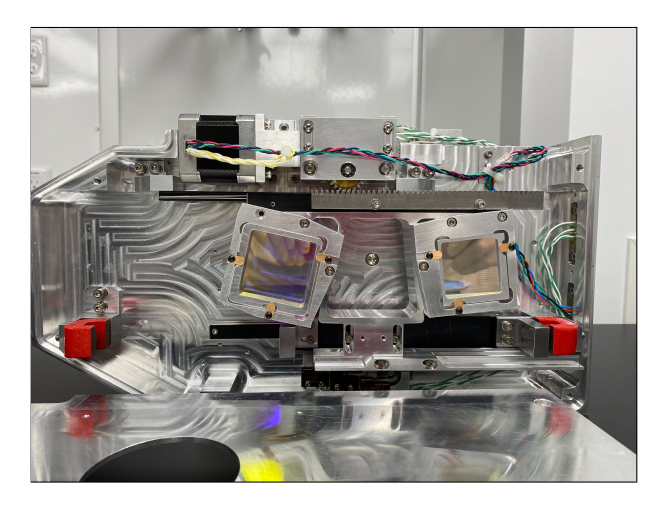


Figure 4. The current prisms and mechanism for aligning the prisms for GPI 1.0. The prisms translate with the metal bar seen along the top, and the magnets (in red) stabilize the positions once the prisms are in place.

motor and coupler, along which the 3 prisms will be shifted along. Because the pitch of the thread of the lead screw is known, the position of the prisms can be ascertained by counting the number of rotations (as turned by the motor). A set of switches on either side of the prism holders is also used as a safety check to determine prism locations just in case.

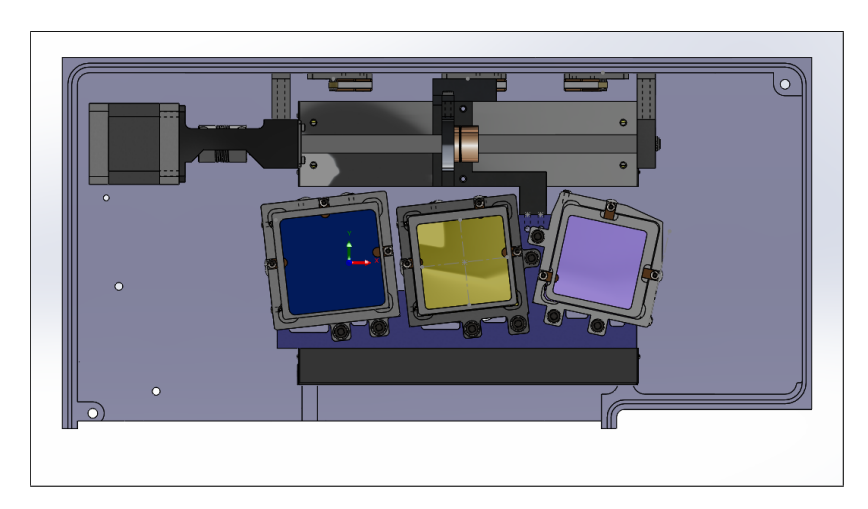


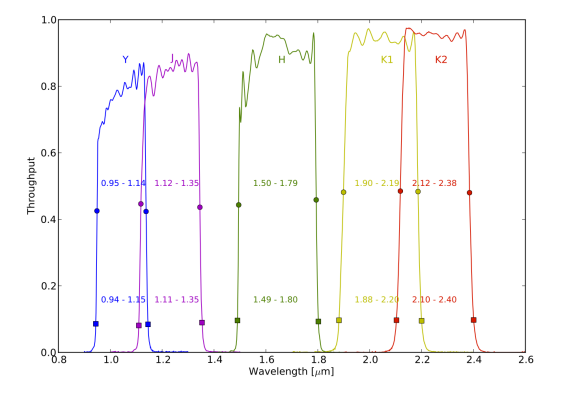
Figure 5. The design for the new prism slide for GPI 2.0; the parts have all been manufactured, and are awaiting assembly/installation. A motor (on the top left of the image) rotates a coupler, which is connected to the lead screw and shifts the prism holders.

6. CHANGES TO THE IFS FILTERS

With the changes to the IFS spectral prisms, the filters had to be updated as well to account for the change in microspectra resolution on the detector. All of the filters besides the H-band filter were upgraded, with the K1 and K2 filters notably being consolidated into a single K band filter. This change has also "normalized" the spectral resolutions of the different bands to be more even. The new filters, manufactured by Asahi Spectra Co. Ltd., provide massive improvements in throughput at the relevant bandpasses while also reducing rippling. The K-band purposefully runs from 2.0 to 2.4 μm . The changes in filter bandpass were done to maximize the bandpass available at each spectral resolution. Operating beyond the standard filter bandpasses were selected by modeling improved signal-to-noise and recovery rate for planetary companions.

Table 2. Filter Band Specifications for GPI 2.0 Filters

	Cut-on Wavelength [nm]	Cut-off Wavelength [nm]
Broadband	970 ± 5	2400 ± 13
Y-Band	950 ± 5	1120 ± 6
J-Band	1100 ± 6	1346 ± 7
H-Band	1500 ± 15	1800 ± 18
K-Band	2000 ± 11	2400 ± 13



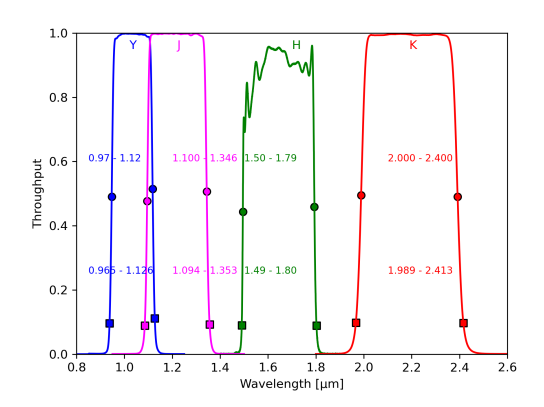
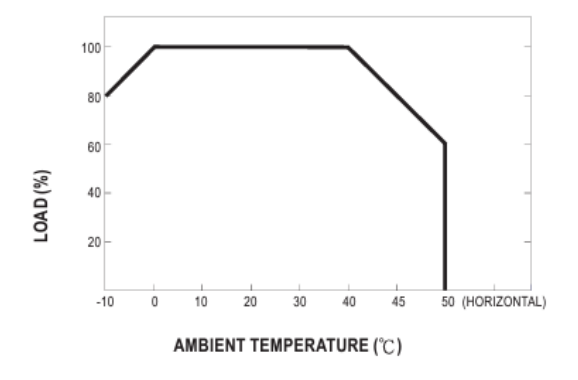


Figure 6. Comparison of the original GPI filter curves(left), and the GPI 2.0 filters (right). Note that the H-band filter has not changed, and that the K1 and K2 filters have been consolidated for GPI 2.0. The circles and squares represent the 20% and 50% transmission wavelengths, respectively. The broadband filter curve is not shown here.

7. IFS ELECTRONIC ENCLOSURE AND RECABLING

The IFS EE has been repackaged to accommodate new electronics and changes made from GPI 1.0 to improve and streamline IFS operation. One of the major changes is that the power supplies for the IFS were swapped for more reliable and efficient units. Essentially direct upgrades over their predecessors, the new power supplies provide the rated load current over a wider range of temperatures while also having a smaller physical footprint for space optimization within the EE.



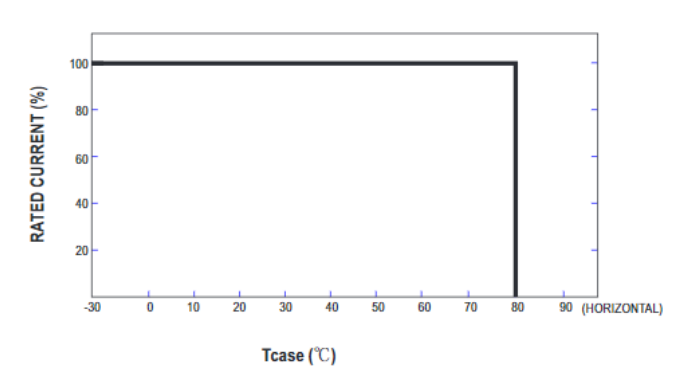


Figure 7. Comparison of load current provided across a range of temperatures of the old (left) Mean Well SP-500-48 [6] and new (right) Mean Well UHP-500-48 [7] power supplies for the IFS. In addition to working over a much larger range of temperatures, the UHP-500-48 is also able to provide 100% of its rated current in its entire operating range.

The IFS EE case was redesigned overall to account for the new inclusion of the Sunpower CCR AVC controllers

(which were previously mounted outside of the EE) and improve airflow. Two additional fans will be mounted along the rear panel, and the rest of the internal components will be rearranged to allow for optimal cooling channels. These changes may help address occasional throttling issues that GPI 1.0 observed with the IFS cryocoolers that could possibly be attributed to derating under heavy loads.

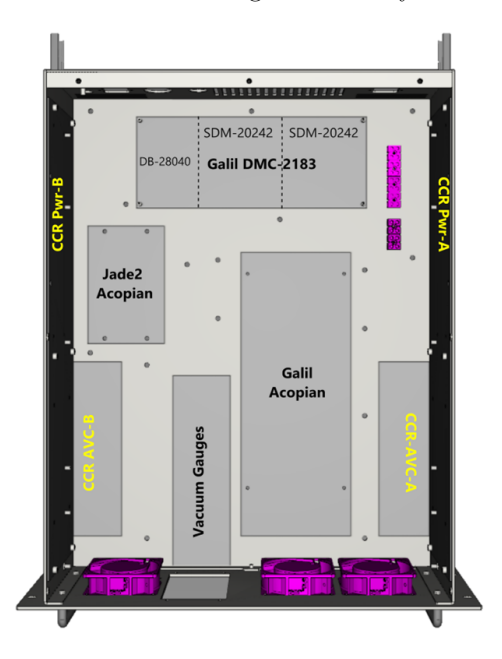


Figure 8. A model of the design of the new IFS EE. The previous components (in grey) have been rearranged to allow for the inclusion of the CCRs and their cables (in yellow), and to maximize airflow.

8. CONCLUSION

The IFS is undergoing a comprehensive suite of upgrades for the transition from GPI to GPI 2.0. Each of these upgrades is intended to increase the scientific output of GPI as a result of lessons learned from the construction of GPI 1.0. Components for most of the systems within the IFS as well as its related electronics have been designed and produced, ready for installation. Once the new parts are successfully integrated into the system, the new Lyot stops, apodizers, prisms, and filters can be tested to fully characterize the performance of the upgrades.

ACKNOWLEDGMENTS

The GPI 2.0 project is supported by a NSF-MRI grant (award AST-1920180) and the Heising-Simons Foundation. The original GPI was supported by NSF grants AST-1411868 and AST-1518332. The international Gemini Observatory is a program of NSF's NOIRLab, which is managed by the Association of Universities for Research in Astronomy (AURA) under a cooperative agreement with the National Science Foundation. on behalf of the Gemini Observatory partnership: the National Science Foundation (United States), National Research Council (Canada), Agencia Nacional de Investigación y Desarrollo (Chile), Ministerio de Ciencia, Tecnologíae Innovación (Argentina), Ministério da Ciência, Tecnologia, Inovações e Comunicações (Brazil), and Korea Astronomy and Space Science Institute (Republic of Korea).

REFERENCES

[1] Nguyen, M. N., Nickson, B. F., Por, E. H., Soummer, R., Hagopian, J. G., Macintosh, B., Chilcote, J., Pueyo, L., Perrin, M., and Konopacky, Q., "GPI 2.0: optical designs for the upgrade of the Gemini Planet Imager coronagraphic system," in [Advances in Optical and Mechanical Technologies for Telescopes and Instrumentation V], Navarro, R. and Geyl, R., eds., 12188, 121884K, International Society for Optics and Photonics, SPIE (2022).

- [2] Greenbaum, A. Z., Cheetham, A., Sivaramakrishnan, A., Rantakyrö, F. T., Duchêne, G., Tuthill, P., Rosa, R. J. D., Oppenheimer, R., Macintosh, B., Ammons, S. M., Bailey, V. P., Barman, T., Bulger, J., Cardwell, A., Chilcote, J., Cotten, T., Doyon, R., Fitzgerald, M. P., Follette, K. B., Gerard, B. L., Goodsell, S. J., Graham, J. R., Hibon, P., Hung, L.-W., Ingraham, P., Kalas, P., Konopacky, Q., Larkin, J. E., Maire, J., Marchis, F., Marley, M. S., Marois, C., Metchev, S., Millar-Blanchaer, M. A., Morzinski, K. M., Nielsen, E. L., Palmer, D., Patience, J., Perrin, M., Poyneer, L., Pueyo, L., Rajan, A., Rameau, J., Sadakuni, N., Savransky, D., Schneider, A. C., Song, I., Soummer, R., Thomas, S., Wallace, J. K., Wang, J. J., Ward-Duong, K., Wiktorowicz, S., and Wolff, S., "Performance of the gemini planet imager non-redundant mask and spectroscopy of two close-separation binaries: Hr 2690 and hd 142527," The Astronomical Journal 157, 249 (jun 2019).
- [3] Peng, D., Curliss, M., Limbach, M. A., Chilcote, J., Hamper, R., Konopacky, Q., Fitzsimmons, J., Macintosh, B., Marois, C., Rantakyrö, F., Aleman, A., Maire, J., Rosa, R. D., Por, E., Savransky, D., Sands, B., Perrin, M., Soummer, R., Kain, I., Pueyo, L., Nickson, B., Nguyen, M., Ó, C. D., Perera, S., and Spalding, E., "GPI 2.0: performance of upgrades to the Gemini Planet Imager CAL and IFS," in [Ground-based and Airborne Instrumentation for Astronomy IX], Evans, C. J., Bryant, J. J., and Motohara, K., eds., 12184, 1218443, International Society for Optics and Photonics, SPIE (2022).
- [4] Chambouleyron, V., Salama, M., Guthery, C., Dillon, D., Perera, S., Konopacky, Q., Wallace, K., Veran, J.-P., Savransky, D., Chilcote, J., Jensen-Clem, R., and Macintosh, B., "GPI 2.0: Implementing a Zernike wavefront sensor for non-common path aberrations measurements," in [Ground-based and Airborne Instrumentation for Astronomy VIII], 12680, International Society for Optics and Photonics, SPIE (2023).
- [5] Limbach, M. A., Chilcote, J., Konopacky, Q., Rosa, R. D., Hamper, R., Macintosh, B., Marois, C., Perrin, M., Savransky, D., Veran, J.-P., Wang, J., and Aleman, A., "GPI 2.0: Upgrades to the IFS including new spectral modes," in [Ground-based and Airborne Instrumentation for Astronomy VIII], Evans, C. J., Bryant, J. J., and Motohara, K., eds., 11447, 1127 1134, International Society for Optics and Photonics, SPIE (2020).
- [6] Mean Well, 500W, Single Output with PFC Function (2012).
- [7] Mean Well, 500W, Slim Type with PFC Switching Supply (2021).